

Forward and inverse problems in fundamental and applied magnetohydrodynamics

Andre Giesecke^{1,a}, Frank Stefani¹, Thomas Wondrak¹, and Mingtian Xu²

¹ Helmholtz-Zentrum Dresden-Rossendorf, P.O. Box 510119, D-01314 Dresden, Germany

² Shandong University, P. O. Box 88, Jing Shi Road 73, Jinan City, Shandong Province, P. R. China

Abstract. This Minireview summarizes the recent efforts to solve forward and inverse problems as they occur in different branches of fundamental and applied magnetohydrodynamics. As for the forward problem, the main focus is on the numerical treatment of induction processes, including self-excitation of magnetic fields in non-spherical domains and/or under the influence of non-homogeneous material parameters. As an important application of the developed numerical schemes, the functioning of the von-Kármán-sodium (VKS) dynamo experiment is shown to depend crucially on the presence of soft-iron impellers. As for the inverse problem, the main focus is on the mathematical background and some first practical applications of the Contactless Inductive Flow Tomography (CIFT), in which flow induced magnetic field perturbations are utilized for the reconstruction of the velocity field. The promises of CIFT for flow field monitoring in the continuous casting of steel are substantiated by results obtained at a test rig with a low melting liquid metal. While CIFT is presently restricted to flows with low magnetic Reynolds numbers, some selected problems of non-linear inverse dynamo theory, with possible application to geo- and astrophysics, are also discussed.

1 Introduction

When a moving electrically conducting fluid comes under the influence of a magnetic field, an electromotive force is produced that drives electrical currents in the fluid which, in turn, modify the original magnetic field. This general principle applies both to the case that a magnetic field is applied from outside, as well as to the case that it is exclusively produced inside the fluid. In the latter case, we speak about self-excitation, or homogeneous dynamo action. It can only occur if the magnetic Reynolds number $Rm = \mu\sigma LV$, i.e. the product of magnetic permeability μ , electrical conductivity σ , size L and velocity scale V of the moving fluid, is significantly greater than one. This condition is well fulfilled in the convecting fluid layers of cosmic bodies, such as the Earth [1] or the Sun [2], but it is much harder to achieve in the liquid metal laboratory. Yet, the threshold of self-excitation has been reached in some dedicated liquid sodium experiments in Riga [3], Karlsruhe [4], and Cadarache [5], and it is

^a e-mail: a.giesecke@hzdr.de

targeted in a few more places around the world [6]. If, however, Rm is not large enough for self-excitation, a magnetic field applied from outside will still be modified by the moving fluid. This effect can be utilized for inferring the velocity field from the externally measured induced magnetic field [7].

In this Minireview, we will deal with both effects: induction under the influence of applied magnetic fields, and self-excitation. We will discuss two mathematical formulations, the first one, the differential equation approach, being based on the induction equation, the second one, the integral equation approach, relying on Biot-Savart's law. In either case, particular attention will be paid to the correct treatment of the boundary conditions for the magnetic field, which is a notorious and non-trivial problem in non-spherical geometries. We will exemplify both methods by treating forward problems related to the French von-Kármán-Sodium dynamo experiment for which we will show that the use of magnetic propeller materials plays a decisive role for the functioning and the mode selection of this type of dynamo [8,9].

The integral equation method is then applied to various inverse induction problems in 2D and 3D. We will show that the Contactless Inductive Flow Tomography (CIFT), as we call it now [7], has a promising potential for the online flow monitoring in technologies such as steel casting or crystal growth. The much harder, since non-linear problem of inverse dynamo theory is only touched upon by discussing some simplified models.

2 Induction and self-excitation: Mathematical basics

In this section we will discuss two different approaches to induction and self-excitation, the first one based on differential equations, the second one on integral equations.

2.1 Differential equation approach

2.1.1 The induction equation

The evolution equation for the magnetic field \mathbf{B} in a fluid of electrical conductivity σ and relative permeability μ_r can be derived from Ampère's law, Faraday's law, the divergence-free condition for the magnetic field, and Ohm's law in moving conductors:

$$\nabla \times \frac{\mathbf{B}}{\mu_0 \mu_r} = \mathbf{j} \quad (1)$$

$$\nabla \times \mathbf{E} = -\frac{\partial \mathbf{B}}{\partial t} \quad (2)$$

$$\nabla \cdot \mathbf{B} = 0 \quad (3)$$

$$\mathbf{j} = \sigma(\mathbf{E} + \mathbf{v} \times \mathbf{B}). \quad (4)$$

In Eq. (2) we have skipped the displacement current because in good electrical conductors the quasi-stationary approximation can be applied. We will also restrict ourselves to the case without external currents. That way, taking the *curl* of Eq. (1) and Eq. (4), and inserting Eq. (2), we obtain the *induction equation* for the magnetic field:

$$\frac{\partial \mathbf{B}}{\partial t} = \nabla \times \left(\mathbf{u} \times \mathbf{B} + \frac{1}{\mu_r \mu_0 \sigma} \frac{\nabla \mu_r}{\mu_r} \times \mathbf{B} - \frac{1}{\mu_r \mu_0 \sigma} \nabla \times \mathbf{B} \right). \quad (5)$$

This is the general form in which spatially varying conductivities and relative permeabilities are taken into account [8], as it will indeed be considered in the later

treatment of the VKS dynamo experiment. If the material parameters are constant in a given volume, the induction equation reduces to the better known simple form:

$$\frac{\partial \mathbf{B}}{\partial t} = \nabla \times (\mathbf{v} \times \mathbf{B}) + \frac{1}{\mu_0 \mu_r \sigma} \Delta \mathbf{B}. \quad (6)$$

The right hand side of Eq. (6) describes the competition between the diffusion and the advection of the magnetic field. Comparing the diffusion time-scale with the kinematic time-scale gives the most important dimensionless number of magnetohydrodynamics, the magnetic Reynolds number $Rm := \mu_0 \mu_r \sigma L V$

Depending on the actual flow pattern, the values of the critical Rm , at which the field starts to grow, are usually in the range of $10^1 \dots 10^3$ [6]. Most flows in cosmic bodies in which Rm is large enough will act as dynamos, although there are a number of anti-dynamo theorems excluding too simple structures of the velocity field or the self-excited magnetic field [10].

Throughout this paper, the velocity field will be considered as given or, in the inverse problems, as an unknown which we will try to reconstruct. That means, in turn, that no attempts will be made to solve the Navier-Stokes equation in the MHD regime.

2.1.2 Simulations in spheres

The easiest geometry for treating the induction equation, together with the demand that \mathbf{B} is curl free in the exterior and vanishes at infinity, is the spherical geometry. Fortunately, planets and stars are in first approximation spherical so that dynamo problems for those bodies are comparably easy to solve.

Considering the solenoidal character of magnetic fields, $\nabla \cdot \mathbf{B} = 0$, and the incompressibility of liquid metals, $\nabla \cdot \mathbf{v} = 0$, both the flow and the magnetic field can be represented in a toroidal-poloidal decomposition:

$$\mathbf{v}(\mathbf{r}) = \nabla \times \nabla \times s(\mathbf{r}) \hat{\mathbf{r}} + \nabla \times t(\mathbf{r}) \hat{\mathbf{r}}, \quad (7)$$

$$\mathbf{B}(\mathbf{r}) = \nabla \times \nabla \times S(\mathbf{r}) \hat{\mathbf{r}} + \nabla \times T(\mathbf{r}) \hat{\mathbf{r}}. \quad (8)$$

Following the Bullard-Gellman formalism [11] the scalar functions s, S, t, T can then be expanded in terms of the spherical harmonics $Y_{m,l}(\vartheta, \varphi)$:

$$S(r, \vartheta, \varphi) = \sum_{l,m} S_{l,m}(r) Y_{l,m}(\vartheta, \varphi) \text{ and } T(r, \vartheta, \varphi) = \sum_{l,m} T_{l,m}(r) Y_{l,m}(\vartheta, \varphi). \quad (9)$$

where we denote the degree and order of the spherical harmonics by l and m , respectively

By inserting Eqs. (7,8) in Eq. (6), multiplying with the conjugate complex $Y_{l,m}^*(\vartheta, \varphi)$, integrating over $d\vartheta d\varphi$, and applying the orthogonality relation of spherical harmonics, one can derive a coupled system of equations for the defining scalars $S_{l,m}(r)$ and $T_{l,m}(r)$ which are second order in r . More details of this procedure can be found, e.g., in [12]. What is interesting in our present context is that the insulating boundary conditions, which require $\nabla \times \mathbf{B} = 0$ in the exterior, lead to two boundary conditions for the scalar fields $S_{l,m}$ and $T_{l,m}$ at the outer radius R that are *diagonal* in l and m :

$$\begin{aligned} \frac{\partial S_{l,m}(r=R)}{\partial r} + l S_{l,m}(r=R) &= 0 \\ T_{l,m}(r=R) &= 0. \end{aligned} \quad (10)$$

It is this diagonality that makes dynamo simulations in spherical geometry quite simple, and the spherical harmonics decomposition was indeed the method of choice for many simulation of cosmic dynamos, but also for the optimization of spherical dynamo experiments such as the MDX experiment in Madison [13].

2.1.3 Treating the boundary conditions for non-spherical domains

The convenient treatment of the boundary conditions, which are diagonal in the degrees and orders of the spherical harmonics, does not extend from spherical to other geometries. For that reason the simulation of liquid sodium dynamo experiments, most of them working in cylindrical geometry, needs significantly higher numerical effort.

For rather compact machines like the Karlsruhe dynamo experiment, with its 52 spin generators and a cylindrical aspect ratio close to one, it appears reasonable to utilize the convenience of spherical harmonics expansion by embedding the actual cylindrical vessel into an enclosing virtual sphere and to assume the space between this enclosing sphere and the real cylinder to be filled with matter of low conductivity. Choosing conductivity factors of 1, 100, and 1000 between the cylinder and the embedding, a convergence towards a realistic critical Rm was obtained in [14].

While this embedding method works reasonably well for cylinders with an aspect ratio close to one, its application to very long dynamos is inconvenient due to the rather slow convergence. Hence, for the Riga dynamo another method has been employed [15,16,17] which is based on the fact that taking the limit $\mu\sigma \rightarrow 0$ the induction equation reduces to a Laplace equation. While in the dynamo region the induction equation is solved, the Laplace equation is solved in the exterior by a pseudo-relaxation method. The solutions in both domains are then matched by appropriate interface conditions for the magnetic field. The scheme has been used extensively for the prediction, optimization and data analysis of the Riga dynamo experiment and the resulting growth rates and frequencies were in remarkable agreement with the experimental ones.

In comparison, the utilization of simplified vertical-field conditions only (i.e., vanishing tangential fields at the boundary, $\mathbf{B}^{\text{tan}} = 0$), turned out to underestimate the critical Rm of the dynamo by some 20 per cent, an error margin that is not acceptable for predictions of expensive liquid sodium experiments.

Another method to treat insulating boundary conditions has been developed in [18,19,20]. The scheme uses a spectral finite element method and was applied successfully to several problems in connection with the VKS experiment [8,21,22] and to precession-driven dynamos in cylindrical domains [23]. The starting point is the fact that the divergence-free and curl-free magnetic field in the non-conducting exterior can be expressed by a gradient of a scalar magnetic potential, according to $\mathbf{B}_{ext} = -\nabla\phi$. Then, the Finite Element approximation for the magnetic field $\mathbf{H} = \mathbf{B}/\mu_r$ in the conducting interior is matched to the solution of the outer Laplace equation by using an Interior Penalty Galerkin method. Typically, the outer spherical insulating domain is made ten times larger than the inner domain so that the concrete form of the boundary conditions at the very outer boundary becomes irrelevant.

A possibility to avoid the solution of the Laplace equation in the exterior is to utilize the mathematically equivalent boundary element method (BEM). This procedure has been proposed in two papers by Isakov et al. [24,25], and was recently modified and applied to various dynamo problems [26,27]. We will present this method in some more detail, since it seems to be most efficient for the simulation of dynamo problems in arbitrary domains.

The method starts with the normal component of the magnetic field at the boundary as obtained from a finite volume method in the interior. The unknown tangential

components of the magnetic field at timestep $(n + 1)$ can then be derived by a matrix operation on a vector composed of the normal components of \mathbf{B} at all surface elements of the computational domain.

The base of the BEM is once again the possibility to express the magnetic field \mathbf{B} as the gradient of a scalar magnetic potential Φ which fulfills the Laplace equation:

$$\mathbf{B} = -\nabla\Phi \quad \text{with} \quad \Delta\Phi = 0, \quad \Phi \rightarrow O(r^{-2}) \text{ for } r \rightarrow \infty. \quad (11)$$

The computation of \mathbf{B} on the boundary therefore requires the integration of $\Delta\Phi = 0$. Consider a volume Ω that is bounded by the surface Γ where $\partial/\partial n$ denotes the derivative in the normal direction: $\partial/\partial n = \mathbf{n} \cdot \nabla$ so that $\partial_n\Phi = -B^n$ yields the normal component of \mathbf{B} on Γ . We can write Greens second identity for the scalar magnetic potential Φ and a test-function G :

$$\int_{\Omega} (G\Delta\Phi - \Phi\Delta G) d\Omega = \int_{\Gamma} \left(G \frac{\partial\Phi}{\partial n} - \Phi \frac{\partial G}{\partial n} \right) d\Gamma. \quad (12)$$

Using $\Delta\Phi = 0$, the potential is determined by the integral expression

$$\Phi(\mathbf{r}) = \int_{\Gamma} \left(G(\mathbf{r}, \mathbf{r}') \frac{\partial\Phi(\mathbf{r}')}{\partial n} - \Phi(\mathbf{r}') \frac{\partial G(\mathbf{r}, \mathbf{r}')}{\partial n} \right) d\Gamma(\mathbf{r}') \quad (13)$$

where $G(\mathbf{r}, \mathbf{r}')$ is the Green's function, or fundamental solution, given by

$$G(\mathbf{r}, \mathbf{r}') = -\frac{1}{4\pi |\mathbf{r} - \mathbf{r}'|} \quad (14)$$

and therefore fulfilling $\Delta G(\mathbf{r}, \mathbf{r}') = -\delta(\mathbf{r} - \mathbf{r}')$. In principle, Eq. (13) is only valid for $\mathbf{r} \notin \Gamma$. For all source points on the boundary the integration domain is enlarged by a small half sphere with the radius ϵ and a short calculation of the limit $\epsilon \rightarrow 0$ results in the boundary integral equation (see e.g. [26]):

$$\frac{1}{2}\Phi(\mathbf{r}) = \int_{\Gamma} \left(G(\mathbf{r}, \mathbf{r}') \underbrace{\frac{\partial\Phi(\mathbf{r}')}{\partial n}}_{-B^n(\mathbf{r}')} - \Phi(\mathbf{r}') \frac{\partial G(\mathbf{r}, \mathbf{r}')}{\partial n} \right) d\Gamma(\mathbf{r}'). \quad (15)$$

From (15) the tangential components of the magnetic field on the boundary $B^t = \mathbf{e}_\tau \cdot \mathbf{B} = -\mathbf{e}_\tau \cdot \nabla\Phi(\mathbf{r})$ are computed by:

$$B^\tau = 2 \int_{\Gamma} \mathbf{e}_\tau \cdot \left(\Phi(\mathbf{r}') \nabla_r \frac{\partial G(\mathbf{r}, \mathbf{r}')}{\partial n} + B^n(\mathbf{r}') \nabla_r G(\mathbf{r}, \mathbf{r}') \right) d\Gamma(\mathbf{r}'), \quad (16)$$

where \mathbf{e}_τ represents the tangential unit vector on the surface element $d\Gamma(\mathbf{r}')$.

A discretization of the equation system (15) and (16) yields an algebraic system of equations which allows for the computation of the (unknown) tangential components of the magnetic field. The discretization of Γ in boundary elements is realized by the tessellation resulting from the finite volume discretization on the domain surface.

2.2 Integral equation approach

An alternative way to deal with the non-local boundary conditions of MHD is the integro-differential formulation developed by Meir and Schmidt [28,29,30]. Using the

current density as the primary electromagnetic variable, it is possible to avoid artificial boundary conditions and fully account for the electromagnetic interaction between flow region and surrounding. The point is that the magnetic field has then to be expressed in terms of the current by Biot-Savart's law. This method is presently being used in a realistic simulation of liquid metal experiment on the so-called Taylor instability, a current-driven kink type instability [31].

Interestingly, this method can be extended into an iterative scheme, by which not only induction effects, but also self-excitation can be treated. Starting with an applied field \mathbf{B}_0 , the authors of [32] search for solutions of the total magnetic field $\mathbf{B} = \mathbf{B}_0 + \mathbf{B}_{ind} = \mathbf{B}_0 + \sum_{k=1}^{\infty} \mathbf{B}_k$, with $\mathbf{B}_k = \mathcal{O}(Rm^k)$. Actually, from a given \mathbf{B}_k they compute the electromotive force $\mathbf{u} \times \mathbf{B}_k$, from which the Poisson equation for the electric potential of the next iteration $\Delta\varphi_{k+1} = \nabla \cdot (\mathbf{u} \times \mathbf{B}_k)$ is derived. From this, the electric current of the $i+1$ iteration is obtained according to $\mathbf{j}_{k+1} = -\nabla\varphi_{k+1} + \mathbf{u} \times \mathbf{B}_k$, and from this current the magnetic field of the $i+1$ iteration is obtained via Biot-Savart's law

$$\mathbf{B}_{k+1}(\mathbf{r}) = \frac{Rm}{4\pi} \int d^3r' \frac{\mathbf{j}_{k+1}(\mathbf{r}') \times (\mathbf{r} - \mathbf{r}')}{|\mathbf{r} - \mathbf{r}'|^3}. \quad (17)$$

Despite the convergence problems of this method when approaching the critical Rm of a dynamo, it is quite helpful to illustrate the various induction processes that enter the dynamo mechanism.

With view on Eq. (17) it is tempting to ask why not to consider Biot-Savart's law as an integral equation for the magnetic field which has to be solved self-consistently. Assuming an infinite domain of homogeneous conductivity, such an approach has been utilized early by Gailitis [33] for the dynamo action of a pair of annular vortices and later by Dobler and Rädler [34] for various dynamo problems.

An extension of such an integral equation method which incorporates the effect of boundaries can already be found in the book of Roberts [35]. However, real use of the method was only made later in the papers [36,37]. With [38] this integral equation method was then extended to the case of unsteady magnetic fields which requires an additional equation for the vector potential \mathbf{A} which is related to the magnetic field by $\mathbf{B} = \nabla \times \mathbf{A}$. The general formulation of the integral equation approach is the following:

$$\begin{aligned} \mathbf{b}(\mathbf{r}) = & \frac{\mu\sigma}{4\pi} \int_V \frac{(\mathbf{u}(\mathbf{r}') \times (\mathbf{B}_0(\mathbf{r}') + \mathbf{b}(\mathbf{r}')))) \times (\mathbf{r} - \mathbf{r}')}{|\mathbf{r} - \mathbf{r}'|^3} dV' \\ & - \frac{\mu\sigma}{4\pi} \int_S \phi(\mathbf{s}') \mathbf{n}(\mathbf{s}') \times \frac{\mathbf{r} - \mathbf{s}'}{|\mathbf{r} - \mathbf{s}'|^3} dS' - \frac{\mu\sigma\lambda}{4\pi} \int_V \frac{\mathbf{A}(\mathbf{r}') \times (\mathbf{r} - \mathbf{r}')}{|\mathbf{r} - \mathbf{r}'|^3} dV' \end{aligned} \quad (18)$$

$$\begin{aligned} \frac{1}{2}\phi(\mathbf{s}) = & \frac{1}{4\pi} \int_V \frac{(\mathbf{u}(\mathbf{r}') \times (\mathbf{B}_0(\mathbf{r}') + \mathbf{b}(\mathbf{r}')))) \cdot (\mathbf{s} - \mathbf{r}')}{|\mathbf{s} - \mathbf{r}'|^3} dV' \\ & - \frac{1}{4\pi} \int_S \phi(\mathbf{s}') \mathbf{n}(\mathbf{s}') \cdot \frac{\mathbf{s} - \mathbf{s}'}{|\mathbf{s} - \mathbf{s}'|^3} dS' - \frac{\lambda}{4\pi} \int_V \frac{\mathbf{A}(\mathbf{r}') \cdot (\mathbf{s} - \mathbf{r}')}{|\mathbf{s} - \mathbf{r}'|^3} dV' \end{aligned} \quad (19)$$

$$\begin{aligned} \mathbf{A}(\mathbf{r}) = & \frac{1}{4\pi} \int_V \frac{(\mathbf{B}_0(\mathbf{r}') + \mathbf{b}(\mathbf{r}')) \times (\mathbf{r} - \mathbf{r}')}{|\mathbf{r} - \mathbf{r}'|^3} dV' \\ & + \frac{1}{4\pi} \int_S \mathbf{n}(\mathbf{s}') \times \frac{\mathbf{B}_0(\mathbf{s}') + \mathbf{b}(\mathbf{s}')}{|\mathbf{r} - \mathbf{s}'|} dS', \end{aligned} \quad (20)$$

where \mathbf{B}_0 is the externally applied magnetic field (which might be zero), \mathbf{b} the induced magnetic field, \mathbf{u} the velocity field, \mathbf{A} the vector potential, ϕ the electric potential and \mathbf{n} denotes the outward directed unit vector at the boundary S . For a steady velocity field, the time dependence of all electromagnetic fields can be assumed to be

$\sim \exp \lambda t$. In (18–20) the temporal variations of the velocity field are ignored, which is justified when the typical diffusive timescale of the magnetic field is shorter than the timescale of velocity variations (which usually is the case in the context of liquid metal experiments).

We have to distinguish three different cases: For non-zero \mathbf{B}_0 , and below the self-excitation threshold, the imaginary part of λ is simply the angular frequency of the applied and also of the induced magnetic field. For $\mathbf{B}_0 = 0$ the equation system (18–20) represents an eigenvalue equation for the unknown time constant λ whose real part is the growth rate, and its imaginary part the angular frequency of the eigenmodes. For $\mathbf{B}_0 = 0$ and $\lambda = 0$, we need only Eqs. (18) and (19) which then reduce to an eigenvalue problem for the critical value of the velocity \mathbf{u} at which the dynamo starts to work.

Note that the integral equation system (18–20) is by far not the only possible one. There are indeed other possible schemes, one of them starting from the Helmholtz equation for the vector potential which leads, however, to a nonlinear eigenvalue problem in λ (see [34]), while the above scheme is a linear eigenvalue problem in λ which has many advantages when it comes to the numerical simulations.

The numerical implementation of the integral equation approach was applied to various dynamo problems [38,39,40,41], and helped also to understand the under-performance of the first VKS experiment in terms of the detrimental role of (rotating) lid layers behind the impellers [39].

3 Forward problems: One example

In this section we will invoke both the differential equation approach and the integral equation approach for understanding the so-called von-Kármán-dynamo (VKS) experiment in Cadarache [5], France.

The working principle of the VKS dynamo is illustrated in Fig 1a. The flow of liquid sodium in a cylinder with diameter 412 mm and height 524 mm is produced by two counter-rotating impellers, each consisting of a massive disk and 8 curved blades. The resulting flow is of the so-called s2+t2 type, which comprises two poloidal eddies, indicated by "s2", with radial inflow (+) in the equatorial plane, and two counter-rotating toroidal eddies, indicated by "t2". This flow topology had been early shown to be a good candidate for dynamo action [42]. In connection with the optimization of the VKS dynamo experiment, Marié, Normand and Daviaud [43] had studied a rather simple analytical test flow of this topological type, which is expressed in the following way:

$$u_r = -\frac{\pi}{2} r (1-r)^2 (1+2r) \cos(\pi z) \quad (21)$$

$$u_\varphi = 4\epsilon r (1-r) \sin(\pi z/2) \quad (22)$$

$$u_z = (1-r)(1+r-5r^2) \sin(\pi z). \quad (23)$$

In order to study dynamo action for this MND-flow, with correctly implementing the vacuum boundary conditions, we had utilized both the differential equation approach (with solving the Laplace equation in the exterior) as well the integral equation approach [39]. For the simplest case without any additional layers around the dynamo, and a toroidal/poloidal ratio $\epsilon = 0.7259$, the structure of the resulting magnetic eigenfield is illustrated in Figs. 1b,c. In Fig. 1b the field lines of the equatorial dipole are seen, while the isosurfaces of the magnetic field energy (Fig. 1c) show the banana-like structure typical for this equatorial dipole eigenmode.

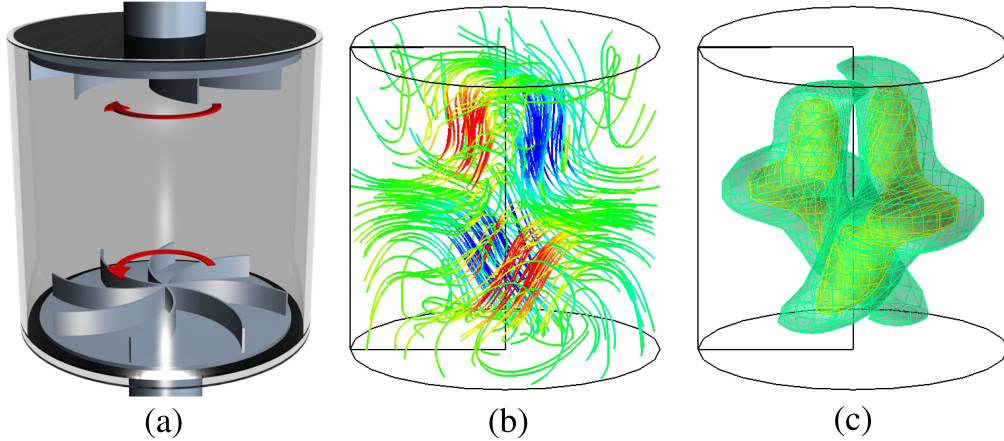


Fig. 1. The VKS dynamo, and its numerical simulation by the integral equation method. (a) Sketch of the experimental setup. The von-Kármán swirling flow is driven by two counter-rotating impellers. (b) Magnetic field lines of the equatorial dipole field resulting for the simplifying MND flow. (c) Iso-surface of the magnetic field energy.

A somewhat surprising results of [39] was that different kinds of layers around the flow field region can have opposite effects on the critical magnetic Reynolds number. While a (stationary) side layer works usually in favor of dynamo action, any layer (stationary or, even worse, rotating) behind the impellers impedes dynamo action significantly. This observation was one of the motivations for the VKS group to replace the non-magnetic impeller material by soft-iron, connected with the idea that such a magnetic material might shield the detrimental induction effects from behind the impellers.

As a result of this modification, dynamo action was indeed observed [5], and subsequent experiments have brought about a remarkable variety of interesting phenomena, including field reversals, excursions, and bursts [44]. Such effects had been neither observed in the Riga nor in the Karlsruhe experiment and thus instigated a strong interest in the geophysics community, with a number of attempts to understand reversals of the geomagnetic field and reversals in the VKS dynamo on the common basis of low-dimensional models [45].

Yet, the basic dynamo mechanism underlying such exciting results remained unexplained for some time. In contrast to all numerical simulations of the VKS dynamo, which had predicted a non-axisymmetric ($m=1$) eigenmode similar to that shown in Fig. 1, the actually observed eigenmode turned out to be more or less axisymmetric and dominated by the toroidal component. Furthermore, the experimentally observed critical Rm around 30 was significantly lower than the predicted one of about 50. The question arose, therefore, whether both effects could be explained by the utilization of magnetic impellers.

In order to answer this question, we have utilized the combined Finite Volume/ Boundary Element Scheme exposed in 2.1.3. With this code we treated a slightly simplified model of the VKS dynamo, in which the bended thin blades were replaced by straight thick ones (see Fig. 2a). Our solutions show two different regimes that differ in the topology of the leading eigenmode. If the relative magnetic permeability of the disks exceeds a threshold of around 20, we observe an interchange of the leading eigenmode from the usual poloidal one to the toroidal one [8]. Yet, this magnetic disk, together with an assumed MND flow in the bulk of the fluid, does not lead to dynamo action, it just gives a toroidally dominated, but still decaying eigenmode (Fig. 2b).

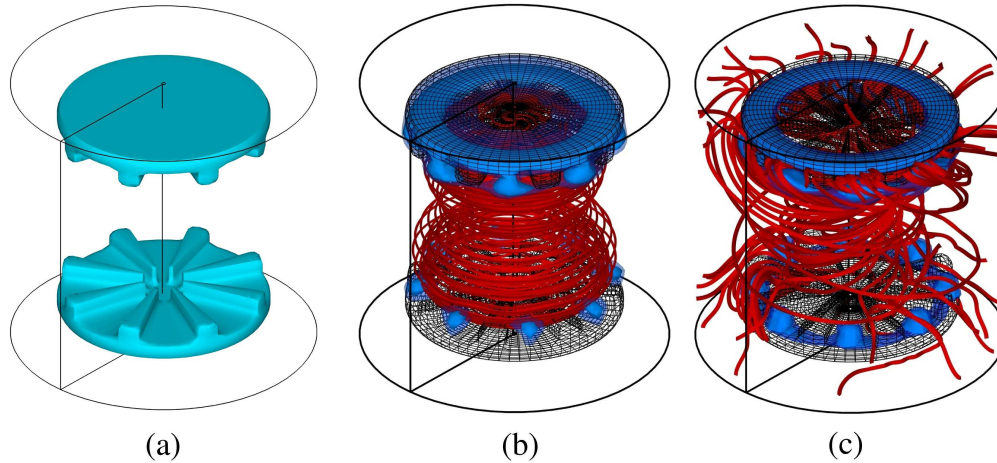


Fig. 2. Effect of the magnetic impellers on the eigenmode selection in the VKS dynamo. (a) Assumed permeability distribution; isolevel at 87.5 percent of the peak value. In the fluid region μ_r is equal to unity. (b,c) Distribution of magnetic energy density and geometric structure of the magnetic field for $\mu_r = 20$. (b) $Rm = 30$, $\alpha = 0$: decaying axisymmetric mode with vanishing poloidal component. (c) $Rm = 30$, $\alpha = -1.5$: Growing axisymmetric mode with poloidal component (after [9]).

What is still needed for dynamo action is some amount of helical turbulence, parameterized by the so-called α effect, which can well be assumed to exist in the space between the blades [47]. This α effect is then able to close the dynamo loop by transforming toroidal field into poloidal field components [9]. The resulting eigenmode, which can now have a positive growth rate, is depicted in Fig. 2c. The experimentally observed eigenmode structure, with its strongly dominant toroidal component, is much in favor of our numerical simulation which explains the functioning of the VKS dynamo by means of strong suction of magnetic flux into domains with enhanced permeability (so called paramagnetic pumping [46]), together with some α effect concentrated between the blades. This example shows that a very detailed treatment of induction effects, with a careful consideration of gradients of material parameters, might be essential for the understanding of experimental results.

4 Inverse problems: Some examples

Assuming a velocity field as given, and asking for the resulting induced (or self-excited) magnetic field, represents a typical forward problem. However, the direction of interest can also be inverted: assume the magnetic field to be known from measurements in the exterior of the fluid, what is then the velocity that produces this field?

4.1 Inverse problems at low Rm

Based on the integral equation system (18-20) in the time-independent limit (i.e. $\lambda \rightarrow 0$), we have developed the so-called Contactless Inductive Flow Tomography (CIFT) for the reconstruction of velocity fields from externally measured magnetic fields [38,48,49,50]. For the case of small Rm , which applies well to many industrial problems like steel casting or silicon crystal growth, the total field $\mathbf{B} = \mathbf{B}_0 + \mathbf{b}$ under

the integrals in (18-19) can be replaced by the applied magnetic field \mathbf{B}_0 alone. This replacement makes the inverse problem of reconstructing the velocity field from the induced electro-magnetic field \mathbf{b} a linear one, which is much easier solvable than the full-fledged non-linear problem with $\mathbf{B} = \mathbf{B}_0 + \mathbf{b}$ under the integrals.

In a first step [48,49], we had shown that, with a vertical field $B_{0,z}$ being applied, the velocity structure of the flow can be roughly reconstructed from the measurement of the induced magnetic field in the exterior and of the induced electric potential at the boundary of the fluid. There remains, however, a non-uniqueness concerning the exact radial distribution of the flow, a fact that can be made plausible by representing the fluid velocity by two defining scalars (for the poloidal and the toroidal velocity component), living both in the whole fluid volume. Then it is clear that two quantities measured only on a two-dimensional covering of the fluid cannot give enough information for the reconstruction of the two desired three-dimensional quantities.

Later, the reconstruction method was advanced to a completely contactless method, CIFT, to avoid the electric potential measurement at the fluid boundary [50]. The main idea was to apply the external magnetic field in two different directions (e.g. $B_{0,z}$ and $B_{0,x}$) and to utilize both corresponding sets of induced magnetic fields for the velocity field reconstruction.

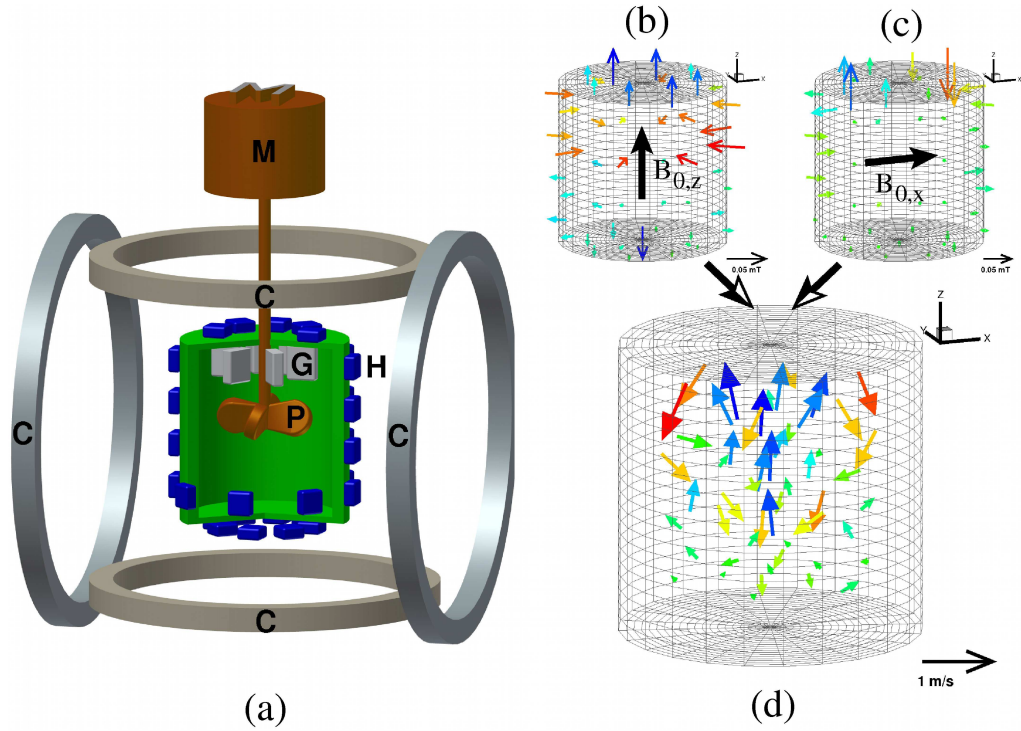


Fig. 3. Application of CIFT to a 3D flow driven by a propeller in a cylindrical vessel. (a) Schematic sketch of the experiment: M - Motor, C - Coils, P - Propeller, G - Guiding blades, H - Hall sensors. (b,c,d) Special case of upward pumping: (b) externally measured induced magnetic fields for applied $B_{0,z}$ and (c) $B_{0,x}$, (d) velocity field as reconstructed from the (b) and (c).

The goal of a first demonstration experiment [38] for CIFT was the reconstruction of a propeller-driven three-dimensional flow of the eutectic alloy GaInSn in a compact

cylindrical vessel with a ratio of height to diameter close to one (see Fig. 3a). In order to determine both the poloidal (in r and z) and the toroidal (in φ) flow components, we applied subsequently a vertical ($B_{0,z}$) and a horizontal ($B_{0,x}$) magnetic field, either produced by Helmholtz-like coil pairs. In this experiment, the switching between the two fields occurs every 3 seconds, so that after 6 seconds all the magnetic field information is available for the velocity reconstruction. Note that this rather poor time resolution can be significantly enhanced, with a physical limitation given by the magnetic decay time, which is in the order of 0.05 s for the demonstration experiment. For each of the two applied fields, $B_{0,z}$ and $B_{0,x}$, the induced fields are measured by Hall sensors at 48 positions, which are rather homogeneously distributed around the surface of the cylindrical vessel. The small ratio of $10^{-3} \dots 10^{-2}$ between the induced and the applied fields demands for a very stable current source of the Helmholtz-like coils, for a very stable relative position of Hall sensors and coils, and for significant effort to compensate drift and sensitivity changes of the sensors.

For the reconstruction of the velocity field we solve the Gauss normal equations that minimize the mean quadratic deviation of the measured from the modeled induced magnetic fields [38]. The intrinsic non-uniqueness problem concerning the detailed depth-dependence of the velocity is overcome by utilizing the so-called Tikhonov regularization by minimizing, in parallel to the magnetic field deviations, also the kinetic energy of the flow or other appropriate quadratic functionals of the velocity. Mathematically, the Tikhonov regularization minimizes the total functional

$$F[\mathbf{v}] = F_{B_{0,x}}[\mathbf{v}] + F_{B_{0,z}}[\mathbf{v}] + F_{div}[\mathbf{v}] + F_{reg}[\mathbf{v}] \quad (24)$$

with

$$F_{B_{0,x}}[\mathbf{v}] = \sum_{i=1}^{N_B} \frac{1}{\sigma_i^2} \left(b_{i,meas}^{(B_{0,x})} - b_i^{(B_{0,x})}[\mathbf{v}] \right)^2 \quad (25)$$

$$F_{B_{0,z}}[\mathbf{v}] = \sum_{i=1}^{N_B} \frac{1}{\sigma_i^2} \left(b_{i,meas}^{(B_{0,z})} - b_i^{(B_{0,z})}[\mathbf{v}] \right)^2 \quad (26)$$

$$F_{div}[\mathbf{v}] = \frac{1}{\sigma_{div}^2} \sum_{k=1}^{N_V} (\nabla \cdot \mathbf{v})_k^2 \Delta V_k \quad (27)$$

$$F_{reg}[\mathbf{v}] = \frac{1}{\sigma_{pen}^2} \sum_{k=1}^{N_V} \mathbf{v}_k^2 \Delta V_k . \quad (28)$$

The two functionals in (25) and in (26) represent, for applied transverse field $\mathbf{B}_{0,x}$ and axial field $\mathbf{B}_{0,z}$, respectively, the mean squared residual deviation of the measured induced magnetic fields $b_{i,meas}^{(B_0)}$ from the modeled fields $b_i^{(B_0)}[\mathbf{v}]$ (that result from the solution of the corresponding forward problem). $F_{div}[\mathbf{v}]$ (Eq. 27) enforces the velocity field to be solenoidal, and $F_{reg}[\mathbf{v}]$ (Eq. 28) is the regularization functional which tries to minimize the kinetic energy. The parameters σ_i in (25) and (26) are the assumed a-priori errors for the measurement of the induced fields. The parameter σ_{div} in (27) is chosen very small as it is a measure for the divergence the velocity solution is allowed to have. The parameter σ_{pen} in (28) determines the trade-off between minimizing the mean squared residual deviation of the observed fields and minimizing the kinetic energy of the estimated velocity field. The normal equations, that follow from the minimization of the functional (24), are solved by Cholesky decomposition. This numerical scheme can easily be extended to incorporate further a-priori information, e.g., the velocity components or mass flow rates known from other measuring techniques.

In the model experiment it was possible to distinguish clearly between upward and downward pumping of the propeller, with the rotational component being reduced by guiding blades in the case of upward pumping. For this case, Figs. 3b,c show the induced fields for applied $B_{0,z}$ and $B_{0,x}$, respectively, and the velocity field as reconstructed from this information (Fig. 3d). The comparison with UDV measurements has shown a good coincidence of the resulting velocity fields (see [38]).

While CIFT is able to infer full 3D velocity fields by applying subsequently two different external magnetic fields, for the following case related to thin slab casting it can be reduced to the determination of the velocity components parallel to the wide faces of the mould [51,52,53]. Figure 4a shows the set-up of the corresponding model experiment Mini-LIMMCAST [54] in which a liquid metal (in our case GaInSn) is poured from a tundish through a submerged entry nozzle into the mould. For this configuration it is sufficient to apply only one magnetic field by a single coil (see Fig. 4a). The interaction of the flow with the applied field produces induced magnetic fields that we measure at 2x7 positions at the narrow faces of the mould in order to reconstruct from them the velocity field. The mathematics of this inversion relies again on the minimization of the mean squared deviation of the measured magnetic fields from the fields according to the integral equation system (18-19). This minimization is done by solving the normal equations, whereby we use various auxiliary functionals which serve to ensure the divergence-free condition of the velocity, to enforce its two-dimensionality, and to minimize in parallel its mean quadratic value, weighted by some regularization parameter.

Figure 4b and 4c show two examples of the reconstructed velocity fields resulting from this inversion. Note that due to the bubbling of argon into the liquid metal at the entrance of the submerged entry nozzle, quite different flow structures can result, such as the desired double vortex flow (Fig. 4b), but also the unwanted single vortex flow as shown in Fig. 4c.

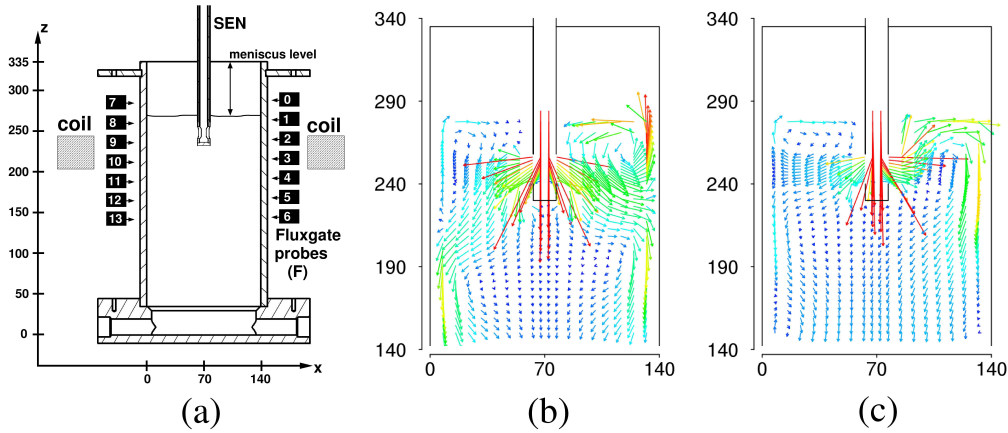


Fig. 4. Application of CIFT to a flow problem related to the continuous casting of steel. (a) Experimental set-up: A liquid metal (GaInSn) is poured through a submerged entry nozzle (SEN) into the mould. Added argon gas leads to a highly chaotic flow in the mould. A magnetic field of about 2 mT is applied by a coil. The flow induced magnetic fields are measured with 2x7 fluxgate sensors at the narrow faces of the mould. (b,c) CIFT reconstructed velocity field in the mould at two different instants, with a double vortex flow (b), and a single vortex flow (c).

4.2 Inverse problems at large Rm

When extending the range of inverse problems from low to large Rm , we have to cope with highly nonlinear inverse problem. Some progress in its treatment has been made for restricted set-ups, for example by applying the so-called frozen-flux approximation for the Earth's core which allows to determine (still with some appropriate regularization) solutions for the tangential velocity field components at the core-mantle boundary from the measured time dependence of the radial magnetic field component [55]. Nowadays, such inversions are augmented by combinations with three-dimensional geodynamo modeling using methods like stochastic inversion [56] or data assimilation [57].

A complementary sort of restricted models is concerned with the determination of the radial dependence of the helical turbulence parameter $\alpha(r)$ from spectral properties, under the (highly artificial) assumption that α is spherically symmetric. Solving such inverse spectral dynamo problems by means of an evolutionary strategy it was possible to obtain such $\alpha(r)$ profiles that lead to oscillatory dynamo solutions [58]. This model was later used to develop simple models of geomagnetic reversals that are just based on noise triggered jumps and relaxation oscillations in the vicinity of spectral exceptional points [59,60,61]. On this basis, a first attempt was further made to infer some of the most essential parameters of the geodynamo, such as its over-criticality and the turbulent resistivity from the temporal behavior and the statistical properties of field reversals [62].

We have to admit, however, that apart from those special solutions with reduced dimensionality, inverse dynamo theory is still in its infancy.

5 Conclusions and prospects

In this paper we have discussed two ways of treating induction problems in magneto-hydrodynamics, one based on the differential equation approach, the other one based on the integral equation approach. We have applied both methods to various forward and inverse problems at small and large magnetic Reynolds numbers.

Much work remains to be done in the field. Concerning the forward problem, the inclusion of time-dependent velocity fields can lead to surprising effects on the thresholds of self-excitation, based on non-normal growth [63] or parametric resonance [64].

As for the inverse problems at low Rm , externally applied fields with different frequencies could in principle be employed for better resolving the velocity field in the depth of the fluid. Likewise, the use of AC fields might give a chance to combine CIFT with other tomographic methods, such as the Mutual Inductance Tomography for the identification of conductivity gradients, as they are connected with the presence of gas bubbles in liquid metals [65].

Inverse dynamo problems will remain a tough nut in the future, with some interesting prospects for inverse spectral methods and data assimilation.

Acknowledgments

We thank Deutsche Forschungsgemeinschaft for financial support in frame of the Collaborative Research Centre SFB 609 (project A5).

References

1. J. Wicht, A. Tilgner, *Space Sci. Rev.* **152**, 501 (2010)
2. C.A. Jones, M.J. Thompson, S.M. Tobias, *Space Sci. Rev.* **152**, 591 (2010)
3. A. Gailitis et al., *Phys. Rev. Lett.* **84**, 4365 (2000)
4. R. Stieglitz, U. Müller, *Phys. Fluids* **13**, 561 (2001)
5. R. Monchaux et al., *Phys. Rev. Lett.* **98**, 044502 (2007)
6. F. Stefani, A. Gailitis, G. Gerbeth, *Zeitschr. Angew. Math. Mech.* **88**, 930 (2008)
7. F. Stefani, Th. Gundrum, G. Gerbeth, *Phys. Rev. E* **70**, 056306 (2004)
8. A. Giesecke, C. Nore, F. Stefani, G. Gerbeth, J. Léorat, W. Herreman, W., F. Luddens, J.-L. Guermond, *New J. Phys.* **14**, 053005 (2012)
9. A. Giesecke, F. Stefani, G. Gerbeth, *Phys. Rev. Lett.* **104**, 044503 (2010)
10. T.G. Cowling, *Mon. Not. R. Astr. Soc.* **140**, 39 (1934)
11. E. Bullard, H. Gellman, *Phil. Trans. R. Soc. London A* **247**, 213 (1954)
12. F. Stefani, A. Giesecke, G. Gerbeth, *Theor. Comp. Fluid Dyn.* **23**, 405 (2009)
13. C.B. Forest et al., *Magnetohydrodynamics* **38**, 107 (2002)
14. K.-H. Rädler, M. Rheinhardt, E. Apstein, H. Fuchs, *Nonl. Proc. Geophys.* **9**, 171 (2002)
15. F. Stefani, G. Gerbeth, A. Gailitis, A., Velocity profile optimization for the Riga dynamo experiment. In: Alemany, A., Marty, Ph., Thibault, J.-P. (eds.) *Transfer Phenomena in Magnetohydrodynamic and Electroconducting Flows* (Kluwer, Dordrecht, 1999), pp. 31-44
16. A. Gailitis, O. Lielausis, E. Platadis, G. Gerbeth, F. Stefani, *Phys. Plasmas* **11**, 2838 (2004)
17. F. Stefani, A. Gailitis, G. Gerbeth, *Astron. Nachr.* **332**, 4(2011)
18. J.-L. Guermond, J. Léorat, C. Nore, *Eur. J. Mech. B/Fluids* **22**, 555 (2003)
19. J.-L. Guermond, L. Laguerre, J. Léorat, C. Nore, C., *J. Comp. Phys.* **221**, 349 (2007)
20. J.-L. Guermond, L. Laguerre, J. Léorat, C. Nore, C., *J. Comp. Phys.* **228**, 2739 (2009)
21. A. Giesecke, C. Nore, F. Plunian, R. Laguerre, A. Ribeiro, F. Stefani, G. Gerbeth, J. Léorat, J.-L. Guermond, *Geophys. Astrophys. Fluid Dyn.* **104**, 249 (2010)
22. A. Giesecke, C. Nore, F. Stefani, G. Gerbeth, J. Léorat, F. Luddens, J.-L. Guermond, *Geophys. Astrophys. Fluid Dyn.* **104**, 505 (2010)
23. C. Nore, J. Léorat, J.-L. Guermond, F. Luddens, *Phys. Rev. E* **84**, 016319 (2011)
24. A.B. Iskakov, S. Descombes, E. Dormy, *J. Comp. Phys.* **197**, 540(2004)
25. A.B. Iskakov, E. Dormy, E., *Geophys. Astrophys. Fluid Dyn.* **99**, 481 (2005)
26. A. Giesecke, F. Stefani, G. Gerbeth, *Magnetohydrodynamics* **44**, 237 (2008)
27. C. Gissinger, A. Iskakov, S. Fauve, E. Dormy, *EPL* **82**, 29001 (2008)
28. A.J. Meir, P.G. Schmidt, *Appl. Math. Comp.* **65**, 95 (1994)
29. A.J. Meir, P.G. Schmidt, *SIAM J. Num. Anal.* **36**, 1304 (1999)
30. A.J. Meir, P.G. Schmidt, S.I. Bakhtiyarov, R.A. Overfelt, *J. Appl. Mech.* **71**, 786 (2004)
31. M. Seilmayer, F. Stefani, T. Gundrum, T. Weier, G. Gerbeth, M. Gellert, G. Rüdiger, *Phys. Rev. Lett.* **108**, 244501 (2012)
32. M. Bourgoin, P. Odier, J.-F. Pinton, Y. Ricard, Y., *Phys. Fluids* **16**, 2529-2547 (2004)
33. A. Gailitis, *Magnetohydrodynamics* **6**, No. 1, 14 (1970)
34. W. Dobler, K.-H. Rädler, *Geophys. Astrophys. Fluid Dyn.* **89**, 45 (1998)
35. P.H. Roberts, *An introduction to magnetohydrodynamics*, (Elsevier, New York, 1967)
36. F. Stefani, G. Gerbeth, K.-H. Rädler, *Astron. Nachr.* **321**, 65 (2000)
37. M. Xu, F. Stefani, G. Gerbeth, *J. Comp. Phys.* **196**, 102 (2004)
38. M. Xu, F. Stefani, G. Gerbeth, *Phys. Rev. E* **70**, 056305 (2004)
39. F. Stefani, M. Xu, G. Gerbeth, F. Ravelet, A. Chiffaudel, F. Daviaud, Léorat, *Eur. J. Mech./B Fluids* **25**, 894 (2006)
40. R. Avalos-Zuniga, M. Xu, F. Stefani, G. Gerbeth, F. Plunian, *Geophys. Astrophys. Fluid Dyn.* **101**, 389 (2007).
41. M. Xu, F. Stefani, G. Gerbeth, G., *J. Comp. Phys.* **227**, 8130 (2008).
42. M.L. Dudley, R.W. James, *Proc. R. Soc. Lond.* **A425**, 407(1989).
43. L. Marié, C. Normand, F. Daviaud, *Phys. Fluids* **18**, 017102 (2006)
44. R. Monchaux et al., *Phys. Fluids* **21**, 035108 (2009)
45. F. Petrelis, S. Fauve, *Phil. Trans. R. Soc. A* **368**, 1595 (2010)

46. W. Dobler, P. Frick and R. Stepanov, *Phys. Rev. E* **67**, 056309 (2003)
47. F. Ravelet, B. Dubrulle, F. Daviaud, P.A. Ratié, *Phys. Rev. Lett.* **109**, 024503 (2012)
48. F. Stefani, G. Gerbeth, *Inverse Problems* **15**, 771 (1999)
49. F. Stefani, G. Gerbeth, *Inverse Problems* **16**, 1 (2000)
50. F. Stefani, G. Gerbeth, *Meas. Sci. Techn.* **11**, 758 (2000)
51. T. Wondrak, V. Galindo, G. Gerbeth, Th. Gundrum, F. Stefani, F., K. Timmel, *Meas. Sci. Techn.* **21**, 045402 (2010)
52. T. Wondrak, S. Eckert, G. Gerbeth, K. Klotsche, F. Stefani, K. Timmel, A. Peyton, N. Terzija, W. Yin, *Metal. Mater. Trans. B* **42**, 1201 (2011)
53. T. Wondrak, V. Galindo, G. Gerbeth, T. Gundrum, F. Stefani, K. Timmel, A. Peyton, W. Yin, S. Riaz, *Ironmaking & Steelmaking* **39**, 1 (2012)
54. K. Timmel, S. Eckert, G. Gerbeth, F. Stefani, *ISIJ Int.* **50**, 1134 (2010)
55. P.H. Roberts, S. Scott, J. Geomagn. Geoelec. **17**, 137 (1965)
56. J. Aubert, A. Fournier, *Nonl. Proc. Geophys.* **18**, 657 (2011)
57. K. Li, P.W. Livermore, A. Jackson, *Phys. Rev. E* **84**, 056321 (2011)
58. F. Stefani, G. Gerbeth, *Phys. Rev. E* **67**, 027302 (2003)
59. F. Stefani, G. Gerbeth, *Phys. Rev. Lett.* **94**, 184506 (2005)
60. F. Stefani, G. Gerbeth, U. Günther, M. Xu, *Earth Planet. Sci. Lett.* **143**, 828 (2006)
61. F. Stefani, M. Xu, L. Sorriso-Valvo, G. Gerbeth, U. Günther, *Geophys. Astrophys. Fluid Dyn.* **101**, 227 (2007)
62. M. Fischer, G. Gerbeth, A. Giesecke, F. Stefani, *Inverse Problems* **25**, 065011 (2009)
63. A. Tilgner, *Phys. Rev. Lett.* **100**, 128501 (2008)
64. A. Giesecke, F. Stefani, J. Burguete, *Phys. Rev. E*, **86**, 066303 (2012)
65. N. Terzija, W. Yin, G. Gerbeth, F. Stefani, K. Timmel, T. Wondrak, A. Peyton, *Flow Meas. Instrum.* **22**, 10 (2011)